Title

Effect of processing conditions on additive DISC patterning of P3HT films

Journal

Journal of Materials Chemistry C, 7(2)

ISSN

2050-7526

Authors

Li, Jun

Holm, Daniella M

Guda, Shravya

et al.

Publication Date

2019-01-03

DOI

10.1039/c8tc04519d

Peer reviewed

Journal of Materials Chemistry C

PAPER

Cite this: J. Mater. Chem. C, 2019, 7, 302

Effect of processing conditions on additive DISC patterning of P3HT films†

Jun Li,[a] Daniella M. Holm,[a] Shravya Guda,[a] Zaira I. Bedolla-Valdez,[a] Goktug Gonel,[a] Ian E. Jacobs,[b]‡ Makena A. Dettmann,[b] Jan Saska,[c] Mark Mascal[c] and Adam J. Moulé*[a]

Received 6th September 2018,
Accepted 1st December 2018

DOI: 10.1039/c8tc04519d

rsc.li/materials-c

There is a critical need to develop a method to pattern semiconducting polymers for device applications on the sub-micrometer scale. Dopant induced solubility control (DISC) patterning is a recently published method for patterning semiconductor polymers that has demonstrated sub-micron resolution. DISC relies on the sequential addition of molecular dopants (here 2,3,5,6-tetrafluoro-7,7,8,8-tetracyanoquinodimethane (F4TCNQ)) to the conjugated polymer. In doped areas, the conjugated polymer is protected from dissolution while in undoped areas, the polymer dissolves into solution. Here we examine factors that affect the resolution of the developed pattern. Two factors are determined to be critical to pattern resolution, the initial crystallinity of the polymer, here poly(3-hexylthiophene) (P3HT), and the quality of the development solvent. We find that dopants diffuse more readily in highly crystalline films than in amorphous films of P3HT and that dopant diffusion reduces the fidelity of the resulting pattern. We also find that the choice of development solvent affects both the fidelity of the pattern and dopant distribution within the patterned polymer domains. Finally, we show that a dopant that diffuses more slowly than F4TCNQ in the P3HT film can be used to pattern the film with higher fidelity. These results together provide a road map for optimizing additive DISC patterning for any polymer/dopant pair.

1 Introduction

Moore's law describes an empirical observation that for the last 50 years the number of transistors on a single integrated circuit has doubled every two years. This remarkable increase in transistor density on Si wafers is due almost entirely to advances in our ability to make lateral and vertical patterns of doped, intrinsic, and dielectric domains at the nanoscale using photolithographic techniques. Thus our ability to pattern semiconductors is responsible for technological progress. Although organic semiconductors (OSCs) are not competitive for computing applications, patterning on the 1–1000 μm scale is valuable for a number of applications. Current applications of semiconducting polymers are, for example, organic light emitting diodes in which pixels of <100 μm's are desired. Also flexible organic transistors with patterning in the 10's of μm range would be desired to control the current to display pixels.[1] Many groups desire to pattern all films to make Hall effect and thermoelectric measurements on the 1–100 μm scale.[2] Cavities for organic lasers require patterning on the μm length scale or less.[3] Defining small active device areas is important in bioelectronic sensing. For example, in a neural sensing device, the area of the polymer is desired to be on the scale of a single cell so that a signal is dominated by a single neuron response.[4]

Recent advances in OSC synthesis and processing have yielded mobility records rivaling and surpassing those of amorphous Si.[5,6] In spite of these remarkable accomplishments, OSCs are not well positioned to enter the commercial device market because there is no equivalent to photolithography to make lateral and vertical nanopatterns of OSCs. There is, therefore, an urgent need to develop new patterning paradigms that are low-cost, rapid, and compatible with OSCs. Solution processing of semiconducting polymers offers a low-cost pathway for high-throughput and large-area coating of devices onto flexible substrates. Advantageous properties such as light weight, chemical tunability, and bio-compatibility make semiconducting polymers an attractive alternative to inorganic semiconductors if the polymer can be printed or patterned with high resolution.

Semiconducting polymers (SPs) are in general incompatible with photoresists because of mutual solubility with solvents

[a] Department of Chemical Engineering, University of California, Davis, California 95616, USA. E-mail: amoule@ucdavis.edu
[b] Department of Materials Science and Engineering, University of California, Davis, California 95616, USA
[c] Department of Chemistry, University of California, Davis, California 95616, USA
† Electronic supplementary information (ESI) available. See DOI: 10.1039/c8tc04519d
‡ Current address: Cavendish Laboratory, University of Cambridge, Cambridge CB3 OHE, UK.

used to apply the resist and the high probability of damage to the polymer when the cross-linked resist is removed.[7] Photolithography using fluorinated resists combined with perfluorinated solvents has been demonstrated.[8] However, multiple layer deposition is difficult due to low surface energy. Also, fluorinated polymer synthesis can be expensive because fluorocarbons are powerful greenhouse gases that destroy ozone and so must be recollected after evaporation in any industrial use.

Deposition of more than 2–3 different materials from orthogonal solvents is in general difficult.[9] Chemical modification of solution OSC materials to enable cross-linking makes patterning of multi-color displays possible, but the chemical modification is difficult, expensive, and can alter the material properties.[10] Ink-jet printing offers an alternative approach for lateral patterning of SPs on the length scale of tens of μm but suffers from several disadvantages including poor definition of pixel edges and formation of non-uniform sample thickness due to the ''coffee stain'' effect.[7,11]

We recently proposed a new SP patterning method called dopant induced solubility control (DISC).[12] DISC relies on the observation that upon doping with a molecular dopant, the SP becomes an organic salt, and thus insoluble in nonpolar solvents. We have developed both additive and subtractive DISC methods. For the additive method, dopants are sequentially evaporated through a shadow mask into the SP. Subsequently, the pattern is developed by dissolving the undoped regions of the SP in a good solvent for the polymer. In an additional sequential processing step, the dopants can be deactivated and removed from the film using a solution of a primary amine (such as propylamine) and a carrier solvent that does not dissolve the polymer, such as acetonitrile.[13] For the subtractive DISC patterning method, the entire film is sequentially doped with a molecular dopant. Next, the film is immersed in an oxygen-containing solvent, such as THF, and illuminated with a 405 nm laser. The laser excites a reaction between the dopant and THF, selectively dedoping the SP that then dissolves into the solvent.[12,14,15] Both methods are compatible with high throughput roll-to-roll (R2R) coating and so need to be carefully explored.

This article details an in-depth study of the additive DISC pattern process for the SP poly-3-hexylthiophene (P3HT) with the molecular dopant 2,3,5,6-tetrafluoro-7,7,8,8-tetracyanoquinodimethane (F4TCNQ) depicted in Fig. 1a. Specifically, we quantify the fidelity of the pattern with respect to the dimensions of the

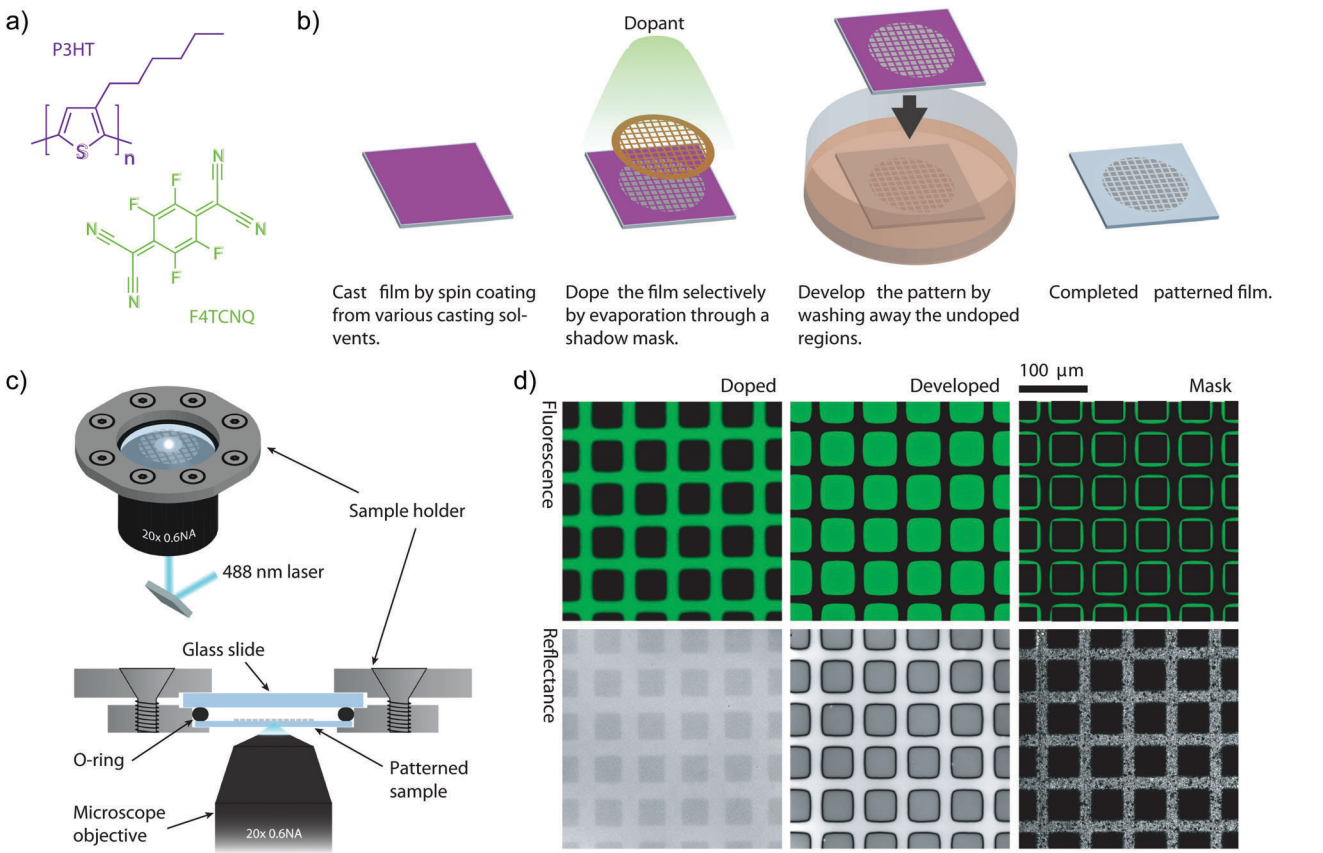

Fig. 1 Sample preparation: (a) molecular structures of P3HT and F4TCNQ. (b) Sequential processing steps to additively pattern P3HT. First the P3HT film is spin coated, then the dopant is evaporated through a shadow mask, next the pattern is developed by immersion in a solvent bath to remove undoped polymer and finally the pattern is completed. (c) Shows the geometry of the sample holder used to measure confocal fluorescence images without O_2 exposure. (d) Example fluorescence and reflectance images of samples after dopant evaporation and pattern development. A reflectance image of the shadow mask is included on the bottom right. Top right is the developed fluorescence image with the area defined by the shadow mask superimposed on the image in black. The green square shows how much larger the developed pattern is than the mask area.

shadow mask. We show that the initial crystallinity of the P3HT has a strong effect on the diffusion rate of the dopant.[16–18] In addition we show that the solvent quality of the developing solvent affects both the patterned layer thickness and etch width. We demonstrate how the initial sample thickness affects the pattern fidelity. Finally, we demonstrate that a higher fidelity pattern can be achieved using alternative dopants.[19] The optimization of these processing parameters can be applied to any combination of SP and molecular dopant for which doping has a large effect on the polymer solubility. We are preparing separate publications on DISC patterning of two different SP/dopant pairs but will restrict this article to P3HT to focus on the relevant processing parameters. Importantly, the additive DISC method is remarkably simple and rapid, which makes high resolution patterning of SPs accessible with little specialized equipment or training.

2 Experimental section

2.1 Materials

P3HT (reported regioregularity >98%, reported M_n = 54–75 kDa), chloroform, chlorobenzene and *ortho*-dichlorobenzene were purchased from Sigma-Aldrich. F4TCNQ was purchased from TCI (98+%). All materials were used as received.

2.2 Sample preparation

One-inch glass substrates (Fisher Scientific) and 25 mm round #1 coverslips (Fisher Scientific) were cleaned by sequential sonication steps in acetone, 10% Mucasol:deionized (DI) water, and DI water, blown dry with compressed nitrogen, and UV-ozone treated for 30 min before use. The substrates were then directly moved into a N_2 glovebox. Solutions of P3HT were prepared at 10 mg ml^{-1} in $CHCl_3$, chlorobenzene (CB), and *o*-dichlorobenzene (ODCB). These solutions were heated overnight at 60 °C to ensure that they were well dissolved. Samples were spin coated to produce ~50 nm film thickness. Thick samples were coated using a higher concentration solution at a slower spin speed. The sample labeled ODCBa was coated from ODCB and then placed directly onto a hotplate heated to 150 °C and annealed for 120 min. The hotplate was then turned off and allowed to cool to room temperature over another hour. All measured samples were then placed simultaneously into a vacuum sample chuck and 400 mesh (38 μm square holes with 26 μm bars) TEM grids (1GN400, nickel) from Ted Pella were attached to the surface using Kapton tape. Next a 3.0 nm F4TCNQ film was deposited onto the films using an MBraun thermal evaporator at a deposition rate of ~0.1 Å s^{-1} at ~80 °C. Next, samples were developed by immersion in a pure solvent bath of either $CHCl_3$, CB, or ODCB at room temperature for 30 s. All fabrication steps were performed inside of a nitrogen glovebox (<3 ppm H_2O, O_2) equipped with a molecular sieve solvent trap.

2.3 Characterization

Before optical microscopy, the samples were sealed into a sample holder designed and machined by the Moulé group to prevent exposure of the sample to O_2 or H_2O. The confocal reflection mode and fluorescence (FL) microscope images were obtained on a Zeiss LSM 700 microscope equipped with a 488 nm laser and a 20× objective with a 0.6 numerical aperture. All images were 16-bit, 2048 × 2048 pixels of 320 μm size. The position of the squares for AFM images was determined by tracking the position of the marked center of the TEM grid. All displayed images are a zoom-in of the original images.

Atomic force microscopy images were obtained in tapping mode on a Digital Instruments Multimode AFM with phase extender module, using BudgetSensor TAP-300G probes.

Fluorescence spectra for calibration were taken on a Varian Eclipse photoluminescence spectrometer with illumination at 550 nm. UV/vis measurements were taken on a Perkin Elmer 700 UV/vis/NIR spectrometer.

3 Results and discussion

3.1 Measuring doping gradients

Fig. 1b shows the additive DISC patterning process. First, a polymer film is coated to a desired thickness. For this publication, all initial P3HT film thicknesses are 50 ± 1 nm unless otherwise noted. Next, F4TCNQ is evaporated under vacuum through a shadow mask onto the polymer film. The shadow mask used here is a 400 mesh zinc TEM grid. Since the polymer film is only 50 nm thick and the lateral features on the shadow mask are tens of μm, we assume that there is no vertical concentration gradient and that F4TCNQ diffuses throughout the vertical depth of the film. Fig. 1c shows the sample holder and measurement geometry that allow us to make confocal fluorescence measurements without exposing the sample to O_2 or H_2O, both of which quench fluorescence in P3HT. As seen in Fig. 1d reflection image, the sample is nearly unchanged after evaporation of the dopant with the only contrast coming from the reduced absorbance of 488 nm light in the doped film. However, the charged dopant and hole on the P3HT are efficient fluorescence quenchers leading to strong contrast in fluorescence microscopy images.[20,21] The fluorescence quenching images are thus an accurate way to determine the concentration of dopants as a function of lateral position. If we compare against a calibration curve of fluorescence intensity *vs.* dopant density we get an absolute measurement of the doping density as function of position.[21] The use of confocal microscopy to track dopant location is simple and could be applied to any SP combined with any p- or n-type dopant or with any molecular acceptor that quenches the fluorescence to determine the density of the small molecule species.

In a subsequent solvent processing step, the sample is immersed in a developing solvent that dissolves the undoped (fluorescing) P3HT but does not dissolve doped P3HT, as shown previously.[12] A reflection image of the completed film now shows strong optical contrast indicating that the undoped P3HT was dissolved. The fluorescence image reveals the doped areas of the polymer, but now this image is shown with a more

sensitive intensity scale than the undeveloped image. The doped polymer is only weakly fluorescing, but we can discern the relative doping density in the features by observing higher fluorescence intensity in pixels with lower dopant concentration. An image of the shadow mask is displayed next to the reflected images. If the area defined by the holes in the shadow mask is placed on top of the developed fluorescence image, then it can be clearly seen that the fluorescing features are larger than the holes defined by the shadow mask. A similar comparison of the feature size in the developed reflectance image also reveals that the patterned P3HT feature is larger than the area defined by the shadow mask. In order for the feature to be larger than the mask, the F4TCNQ dopant must have diffused laterally within the P3HT layer for a distance of $>\mu$m. We have previously reported that F4TCNQ can diffuse in P3HT with thermal activation using similar experiments.[21] The large diffusion distance seen here shows that the initial diffusion rate during evaporation (first seconds) is significantly higher than the diffusion rate once the dopants have been introduced to the film (minutes to weeks).

The results in Fig. 1d must be addressed on several levels. First: what is the mechanism that allows long-range diffusion of dopants within the P3HT film during evaporation? Second: how do properties of the P3HT film, like initial crystallinity or doping level, affect the diffusion rate and distance? Third: how does the developing step affect the fidelity of the pattern?

In order to address these questions, we systematically changed the initial crystalline order of the P3HT film by spin coating the P3HT film from a series of casting solvents that decrease the drying rate and thus increase the crystallization time for P3HT. As has been previously reported, changing the casting solvent from chloroform ($CHCl_3$) to CB to ODCB increases the time necessary for the P3HT film to form and thus increases the crystalline order after spin coating.[22–25] We also thermally annealed an ODCB cast sample at 150 °C for 120 min and allowed it to slow cool (ODCBa) to induce even further crystalline order. With longer drying time the first vibronic absorbance peak at 610 nm increases while simultaneously the amorphous absorbance at 450 nm decreases (Fig. S1, ESI†). These optical changes are consistent with more highly ordered P3HT chains and reduced amorphous content and thus consistent with the claim that longer drying time increases the crystallinity of P3HT films.[24,26,27] We note that halogenated solvents are not necessary and for a scaled-up process should be replaced with less toxic alternatives.

Our expectation, prior to experimentation, was that increased crystalline order in the P3HT would reduce the diffusion rate of the dopant laterally through the film because the crystalline domains would block the diffusion. Fig. 2a shows confocal fluorescence images of undeveloped samples prepared using the method shown in Fig. 1b. All four samples were placed into the evaporator simultaneously and were rotated above the evaporation source, meaning that all samples received identical amounts of F4TCNQ. All four samples also have nearly identical thickness (50 ± 1 nm). The fluorescence images of the undeveloped samples show that the grid pattern that was covered by the mask has the

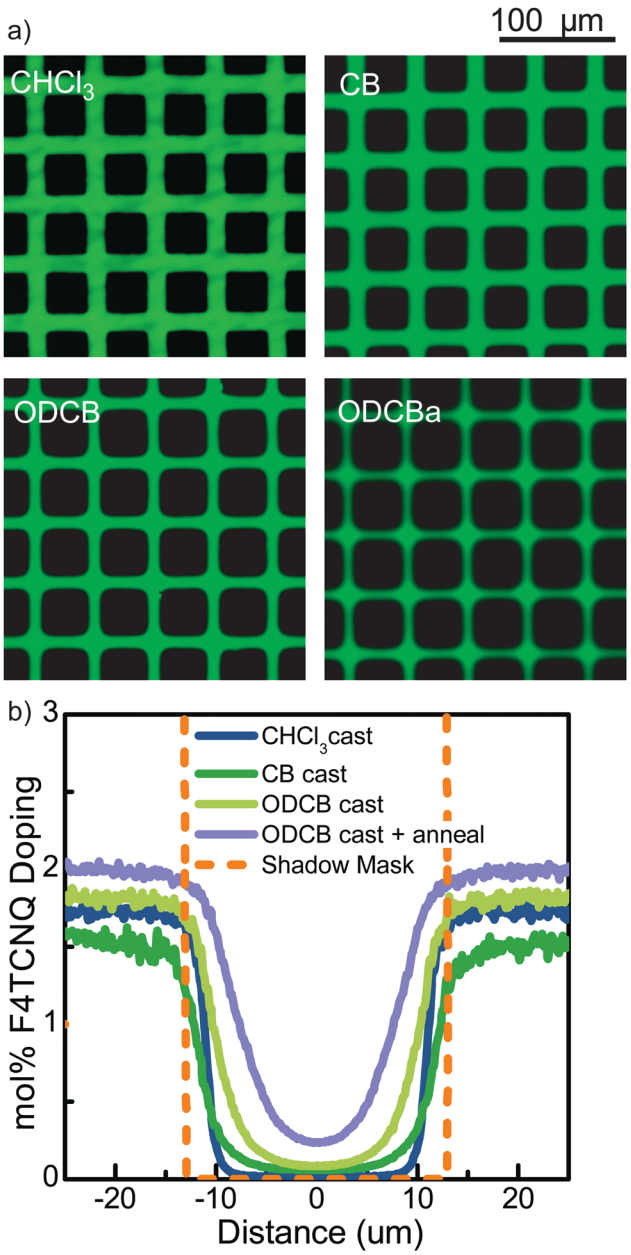

Fig. 2 Imaging dopant location: (a) confocal fluorescence images of undeveloped patterned samples that were coated from $CHCl_3$, CB, ODCB, and ODCB + thermal annealing. (b) F4TCNQ doping concentration *vs.* position for undeveloped samples as calculated from fluorescence images and compared to the mask dimension.

widest features for the $CHCl_3$ cast sample and progressively narrower features for CB → ODCB → ODCBa cast samples. This result means that prior to development, the diffusion distance of the F4TCNQ increases proportional to the crystallinity of the P3HT, opposite to the expected trend.

Fig. 2b shows a plot of the mol% of F4TCNQ in P3HT as a function of position across the masked feature for all four coating conditions. The amount of the dopant is calculated using a calibration curve for the fluorescence *vs.* concentration. This calibration curve is based on samples prepared from

P3HT/F4TCNQ solutions with known mixing ratio and coated from CB.[28] The sample crystallinity and doping level both have a strong effect on the fluorescence intensity in P3HT. This means that the absolute doping concentration for other coating conditions have a systematic error with unknown sign. However, the plots do convey the relative doping level as a function of position. This data shows that F4TCNQ diffuses laterally in all of the samples by several μm. The data also makes clear that F4TCNQ diffusion is higher in ODCB cast and ODCB cast + annealed samples than lower crystallinity samples coated from $CHCl_3$ or CB.

In a previous publication, we quantified the thermally activated diffusion rate of F4TCNQ in P3HT films using P3HT/F4TCNQ samples with geometry identical to the undeveloped sample geometry.[21] In order to fit the diffusion rate we needed to include two diffusing species (F4TCNQ and $F4TCNQ^-$) into our model. The local ratio of $F4TCNQ^-$ to F4TCNQ depends on the number of occupied doping sites in the amorphous P3HT assuming a Langmuir isotherm model for site filling.[28] We found that $F4TCNQ^-$ does not drive diffusion from high concentration to low concentration regions in P3HT because the jump distance per jump attempt is very low for $F4TCNQ^-$. Instead, macroscopic diffusion is caused mostly by diffusion of neutral F4TCNQ, even though it is a minority species. Also, the jump distance of neutral F4TCNQ is much larger in highly doped regions of the P3HT because there are not many available (unoccupied) sites for the F4TCNQ to re-dope the sample.[21] We calculated that if a film of P3HT is coated from CB and sequentially doped from a solution of F4TCNQ in acetonitrile, that the saturation number of available doping sites in P3HT is 4.9 mol%.[28] We also showed that sequential doping from solution placed F4TCNQ into amorphous domains only and did not disturb the structure of crystalline domains.[28] These results have been verified recently by Chew *et al.*[27]

Here we assume that the saturation doping level for P3HT cast from CB is the same when comparing sequential doping from a thermally evaporated F4TCNQ *vs.* sequential solvent doping. We hypothesize that the number of unoccupied doping sites is inversely proportional to the vol% of P3HT in crystalline domains. This is because only amorphous domains are doped and there is a smaller volume fraction of amorphous domains if the sample is more crystalline. Thus if the as-cast sample has increasing crystallinity with longer drying times $CHCl_3$ → CB → ODCB → ODCBa, then the number of doping sites per unit volume will follow an opposite trend. There are fewer available doping sites per volume in P3HT coated from ODCBa than ODCB than CB than $CHCl_3$ cast samples.

The cartoon in Fig. 3 summarizes the findings from the undeveloped sample data combined with previous results on doping P3HT with F4TCNQ. The F4TCNQ diffused farthest in the high crystallinity ODCBa sample because there was the lowest density of available doping sites. The neutral F4TCNQ, introduced to the sample through the mask, diffused laterally until it found empty doping sites and became ionized to $F4TCNQ^-$. In contrast, more doping sites are available per unit volume in the less crystalline $CHCl_3$ cast sample so the F4TCNQ

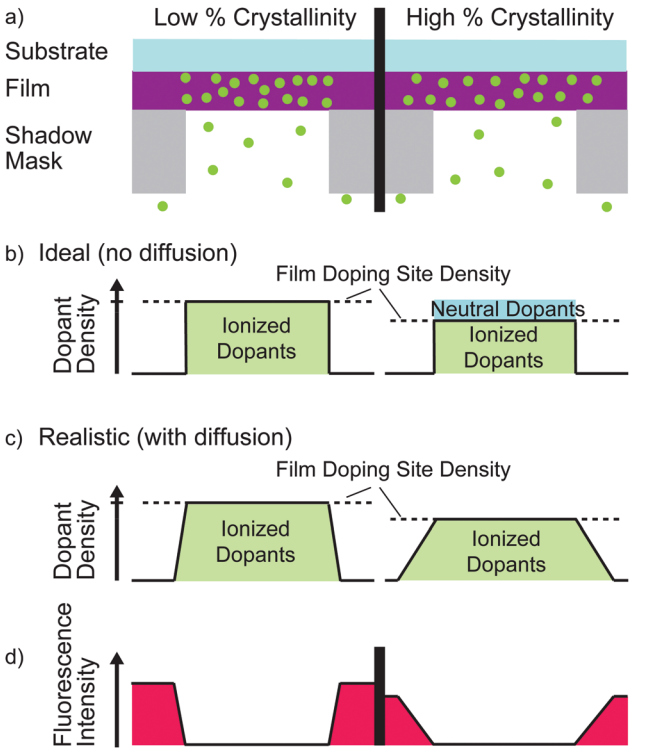

Fig. 3 Effect of crystallinity on dopant location: (a) cartoon depicting dopants being evaporated through a shadow mask into a polymer layer. A more crystalline film has a lower volume fraction of amorphous sites that can be doped. (b) shows the ideal (no diffusion) distribution of ionized dopants. (c) Realistically, neutral dopants will diffuse until finding an available doping site, allowing greater diffusion under the mask in more crystalline films. (d) The fluorescence intensity matches the density of amorphous sites that are not occupied by dopants.

did not diffuse as far into the undoped region covered by the mask. The extent of the diffusion is observed using the fluorescence intensity. Bringing these ideas together, if more dopants per area are introduced than can be accommodated into the available doping sites per volume, then the excess neutral dopants will diffuse laterally and bleed out of the desired (masked) area. To maximize the pattern fidelity, it is therefore critical to match the density of introduced dopants to the available doping site density. Determining the density of available doping sites is not easy, as shown here, because the density of doping sites in the polymer depends on intrinsic features of the polymer such as molecular weight, polydispersity, and regio-regulatity. Even within a uniform polymer sample, doping site density is affected by processing conditions such as coating solvent, solvent evaporation rate, and post coating thermal processing.

3.2 DISC patterned samples

In this section we explore how the distribution of dopants and crystallinity of the undeveloped sample affects the sharpness of the developed pattern and the distribution of dopants within the patterned domains. Fig. 4a shows confocal fluorescence and reflectance images of developed P3HT/F4TCNQ samples. From left to right the samples are arranged to depict samples

that were coated with increasing crystallinity ($CHCl_3$ → CB → ODCB → ODCBa), meaning that the dopants spread further under the mask. From top to bottom the samples are arranged to show increasing solvent quality ($CHCl_3$ → CB → ODCB) of the developing solvent for P3HT. The solubility of P3HT in any solvent depends heavily on the M_w, PDI, and regio-regularity of the sample.[29–32]

The reflectance images show a flat background and darker squares that are patterned doped polymer domains defined by the mask. Reflectance microscopy is a simple method to quickly determine how well the pattern formed over large areas. However, reflectance measurements do not allow determination of the patterned sample thickness and are difficult to interpret quantitatively. For example, each polymer feature has a dark ring around the outside that comes from scattering of incident light from the border of the feature. In order to quantitatively examine the size and shape of patterned features, we used atomic force microscopy (AFM) in tapping mode to make zoomed-in topography images of the patterned samples. These topography images are shown in Fig. 4b alongside the same features imaged using fluorescence microscopy.

While the AFM image depicts the material on the substrate with full height information, fluorescence microscopy gives information about the dopant density within the P3HT film. Particularly in the samples developed using $CHCl_3$, the fluorescence images show a ring of high fluorescence intensity around the border of the patterned features. We attempted to calculate the doping density as a function of position using fluorescence similar to Fig. 2b. However, it was not possible because, unlike in the undeveloped sample, the fluorescence in the developed sample comes from a sample that changes both thickness and dopant density as a function of position. In addition, the development solvent changes the P3HT crystallinity and allows the dopant to intercalate into crystalline domains,[28,33] which

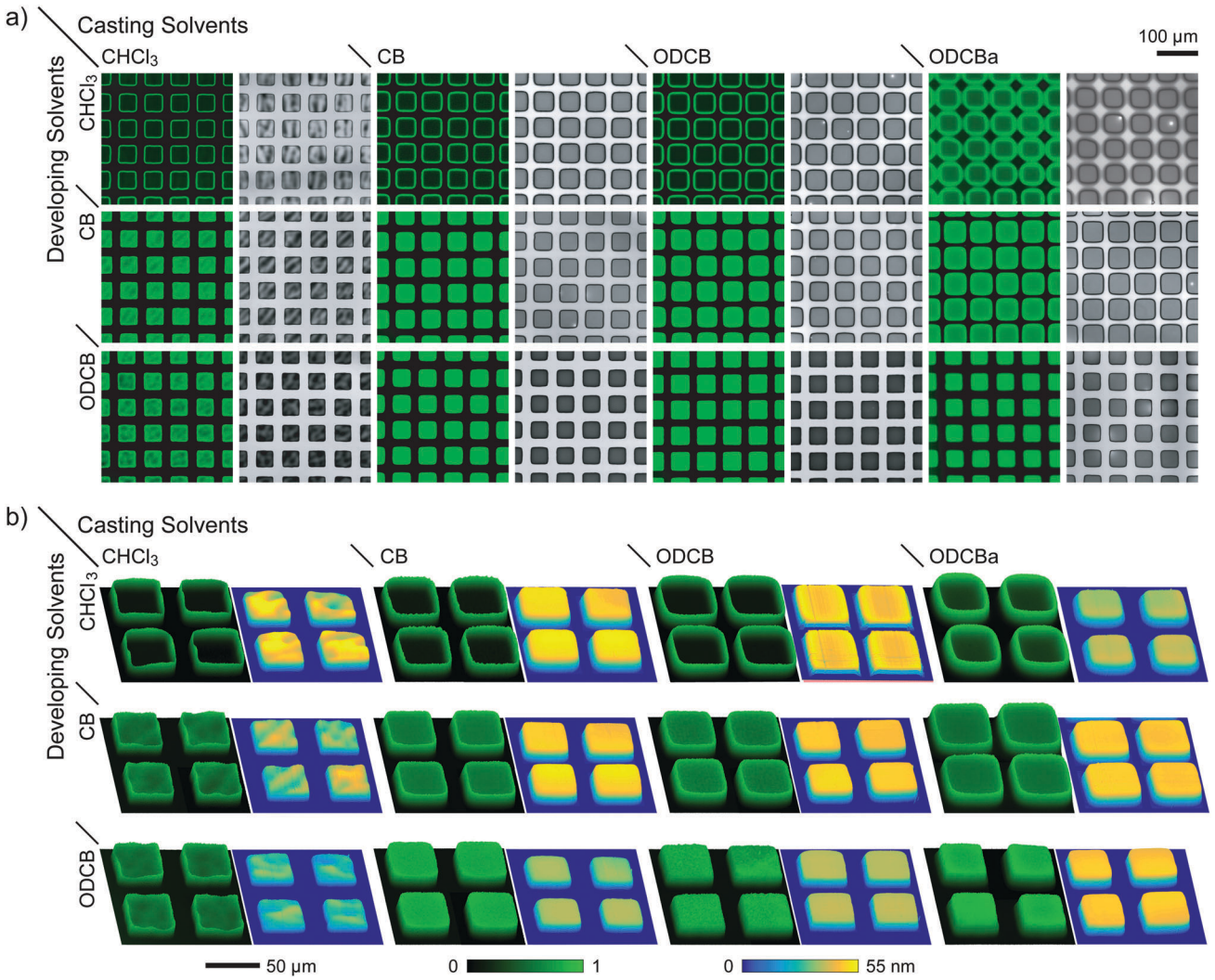

Fig. 4 Imaging developed samples: (a) fluorescence and reflection images of developed samples that were coated with increasing solvent quality ($CHCl_3$ → CB → ODCB → ODCBa) to yield higher initial crystallinity and developed with increasing solvent quality ($CHCl_3$ → CB → ODCB) to yield a more aggressive solvent etch. (b) The same fluorescence imaging data at higher resolution and AFM images of the same sample area. The reflectance and AFM images quantify the location of the polymer while the fluorescence image depicts the relative doping level within each polymer sample.

makes the fluorescence calibration curves invalid. Finally, there are small but important differences in the pixel size and spacing between the AFM and confocal fluorescence images that come from systematic errors such as drift of the piezos in both instruments. The combination of thickness change, solvent exposure, and image alignment leads to unacceptably high uncertainty in the calculation of the dopant density. Instead, we interpret the fluorescence images as showing the relative dopant density as a function of position.

To understand the combined quantitative effects of initial P3HT crystallinity and development solvent quality on the pattern fidelity, we examine averaged cross-sections of negative (developed) features from the AFM images. The cross-sections are taken from multiple different features and averaged over the 1 μm nearest to the center of the feature (furthest from the corners). Fig. 5 shows a selection of the full cross-section data, with the rest in Fig. S2–S6 (ESI†). Fig. 5a shows AFM cross-sections from samples that were coated from CB and developed from $CHCl_3$, CB, and ODCB. These samples all have identical initial P3HT crystallinity (same as Fig. 2a) but clearly different feature dimensions after being developed. Here it is clear that the F4TCNQ diffused through the P3HT for several μm under the mask even though the diffusion rate of F4TCNQ in P3HT at room temperature is negligible over hours.[21] With increasing solvent quality the width of the feature increases because the higher quality solvent is able to dissolve P3HT with a higher doping level. At the same time, increasing solvent quality results in reduction of the polymer feature height because a good solvent is able to remove low M_w chains from the doped portions of the film, while a poorer solvent like $CHCl_3$ does not result in any thickness loss. Thus the choice of developing solvent quality is critical for pattern fidelity because the film thickness change and feature width must be balanced.

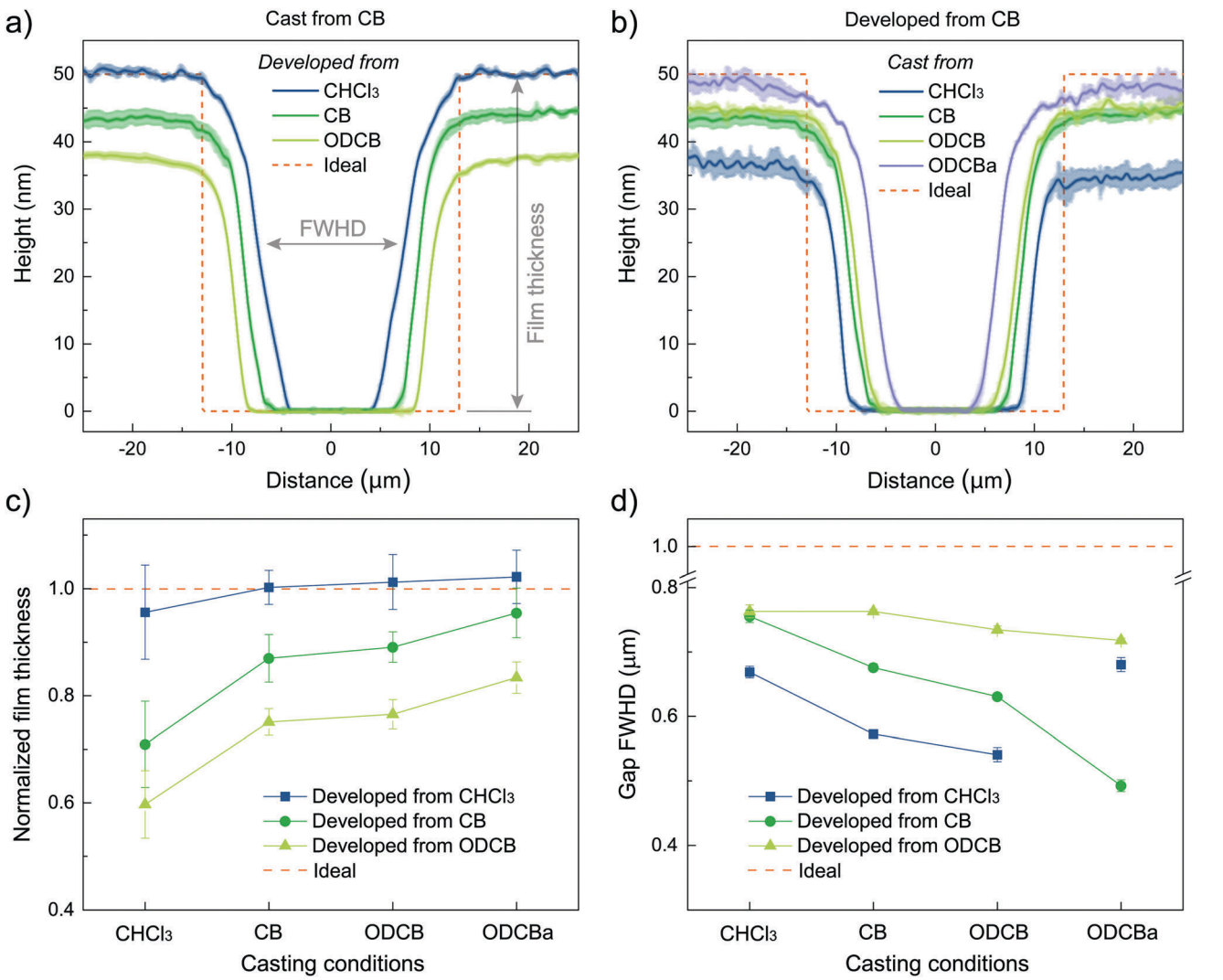

Fig. 5 Pattern fidelity: (a) plot of height above the substrate *vs.* lateral distance for an averaged line profile through AFM images of films developed using various solvents that were coated from CB solutions. The orange dotted line depicts the feature size expected from precise etching of the shadow mask. (b) Similar height profiles as in (a) but for samples coated using various solvents and developed using CB. (c) Plot of normalized layer thickness of all samples coated and developed using all solvents. (d) Plot of the etched feature width at $\frac{1}{2}$ of the film thickness for all samples coated and developed using all solvents.

Fig. 5b shows cross-sections of films coated from solvents that lead to different initial crystallinity and thus F4TCNQ diffusion distance, but are all developed from CB. Again the comparison of these samples leads to a predictable trend. As demonstrated in Fig. 2b and 3, F4TCNQ diffuses farther under the mask in P3HT samples with higher initial crystallinity and so these samples have a narrower negative feature than samples with low initial crystallinity. Alternatively, samples that have higher initial crystallinity are less soluble and short chain polymers are more likely to be entangled in crystalline domains so these samples lose less thickness upon development than samples with lower initial crystallinity. Thus there is a trade off between layer thickness and feature width. Highly crystalline samples have high dopant diffusion, compromising pattern fidelity, but low solubility on development, preserving the doped film thickness.

Fig. 5c and d summarize the change in normalized thickness of the DISC patterned features that occurs from development and the full width at half depth (FWHD) of the negative features for all twelve combinations of casting and development solvents. All conditions show a clear trend with both development solvent quality and initial crystallinity except the film coated with ODCB and annealed (highest initial crystallinity) and developed with $CHCl_3$ (lowest solvent quality). This sample was so insoluble that the undoped polymer behind the mask did not dissolve completely during development and so represents an outlier point.

The change in film thickness and negative feature FWHD are a good starting point for analysis of the pattern fidelity but neither measure accounts for the shape of the patterned feature. In order to analyze the shape of the negative feature, we took derivatives of the AFM height profiles depicted in Fig. 5 and Fig. S6 (ESI†). An example of this derivative is depicted in Fig. S7 (ESI†) and shows a slope of zero on the top of the positive feature and at the substrate surface and negative and positive peaks (from left to right) representing the change in height as a function of lateral position. The important information that can be extracted from this analysis is the magnitude of the derivative peak that corresponds to the highest slope or sharpest vertical etch and the full width at half maximum (FWHM) of the derivative that represents the sharpness of the etch interface (lateral distance over which a change in height occurs). Table 1 presents peak value and FWHM of the height derivative averaged over many feature edges for all twelve combinations of initial crystallinity and development solvent quality. Maximizing the peak value of the etch derivative means that the combination of deposition and development solvents yields a particularly sharp etch. Interestingly, the highest slope is reached under processing conditions in which the development solvent is the same as the coating solvent. If the FWHM of the etch derivative is minimized, this indicates that the change in slope occurs over the smallest lateral distance, which is a quantification of the etch sharpness. Again for this measure, the sharpness of the P3HT pattern is maximized when the coating solvent and the development solvent are the same. We can conclude from this analysis that using the same coating and development solvents causes the formation of the sharpest etch features in the additive DISC process.

Analysis of the confocal microscopy images gives an insight into the relative doping density within the developed features. It is clear from Fig. 4 that many of the samples have a ring of increased fluorescence around the edge of the etched features that corresponds to reduced doping density. Fig. 6 shows averaged cross-section profiles of the fluorescence intensity across a negative etch feature for samples coated from all four conditions and developed using CB. Fig. 6a shows the fluorescence intensity in total counts while Fig. 6b shows normalized data. All of the fluorescence intensity profiles have low fluorescence intensity in the doped and flat positive features, a peak in fluorescence intensity near the feature edge and then no fluorescence in the negative etch.

The right side of Fig. 6b shows a clear trend in the data when comparing samples. The maximum fluorescence occurs within the edge of the height feature seen in the AFM images above. This shows that the positive fluorescence feature comes from P3HT near the border of a square that is doped to a lower degree than directly beneath the hole in the mask but still high enough to reduce the solubility and remain undissolved.

Fig. S8 and S9 (ESI†) show all of the fluorescence cross-sections, both raw and normalized, organized for samples with differing casting solvent and the same development solvent (Fig. S8, ESI†) and for identical casting solvent and differing development solvent (Fig. S9, ESI†). In general, samples developed using $CHCl_3$ have a much higher intensity ring of fluorescence than the other development solvents and the ring tends to be closer to the middle of the negative etch feature.

Fig. 7 is a schematic that explains how the combination of doping level and solubility generates the varying intensity of the fluorescence ring. At the top is a generic interface with a doping level that changes from high to low across the interface from the mask edge. In an undeveloped sample, the fluorescence

Table 1 Quantification of pattern fidelity: the derivative of each cross-section was analyzed for the peak values of the edge derivative and the FWHD of the edge derivative. Bolded values reveal the coating conditions that yield the etch pattern that best matches the shadow mask for each developing solvent

	Peak values of edge derivatives ($\times 10^{-3}$)				FWHM of edge derivatives (μm)			
Developed from	Cast from $CHCl_3$	Cast from CB	Cast from ODCB	Cast from ODCBa	Cast from $CHCl_3$	Cast from CB	Cast from ODCB	Cast from ODCBa
$CHCl_3$	**18.07 ± 1.46**	8.67 ± 0.03	10.12 ± 1.90	2.57 ± 0.23	**1.80 ± 0.73**	5.23 ± 0.02	3.68 ± 0.98	8.93 ± 2.22
CB	13.32 ± 0.19	**12.66 ± 0.75**	9.71 ± 0.03	12.43 ± 0.52	2.35 ± 0.09	**3.01 ± 0.04**	4.42 ± 0.36	3.17 ± 0.10
ODCB	10.65 ± 0.21	9.51 ± 0.59	**11.24 ± 0.26**	**13.62 ± 0.65**	2.34 ± 0.10	3.62 ± 0.14	**3.03 ± 0.06**	**2.75 ± 0.06**

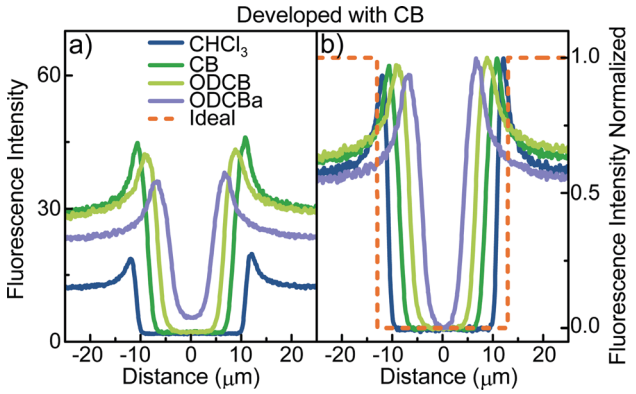

Fig. 6 Relative doping density: averaged profiles of the confocal fluorescence intensity as a function of lateral distance for samples coated using all conditions and developed using CB. (a) Depicts raw fluorescence and (b) shows fluorescence intensity normalized to the highest intensity for each condition.

intensity would increase in inverse proportion to the doping level. The solubility of the film is also inversely proportional to the doping density. Vertical dotted lines are added to show the solubility cutoff as a function of doping level for ODCB, CB, and $CHCl_3$. Assuming that this interface were to be developed with these three solvents, the best solvent would produce the most aggressive etch as seen in Fig. 5. The width of the etch feature for a developed sample is depicted using colored bars coded for the three solvents. The developed sample fluorescence intensity is the product of the developed sample thickness and projected undeveloped sample fluorescence intensity. This product shows why there is little or no peak in fluorescence for a film developed with ODCB. The good solvent dissolved all of the undoped polymer and most of the weakly doped polymer, leaving little material than can emit light. Alternatively, for samples developed with $CHCl_3$, a very low doping level is sufficient to render the sample insoluble, so there is a lot of material remaining that can fluoresce. The thickness variation across the interface yields a peak in the fluorescence as seen in Fig. 6.

3.3 Other factors affecting patterning fidelity

In this section we will discuss other processing parameters that can affect the pattern fidelity using the additive DISC process. So far, this article has focused on how the initial crystallinity of the film, controlled using the casting solvent, and the quality of the developing solvent, affect the resulting pattern. Here we comment on the M_w distribution of the polymer, the film thickness, dopant concentration, and the dopant used. As mentioned above, the M_w distribution and regio-regularity of the polymer sample has a large effect on the polymer solubility.[29,30,32] In the samples depicted here, those developed with CB or ODCB lose thickness. This is due to the relatively low regio-regularity (90%) and large M_w distribution (5–80 kDa) of the regular grade P3HT purchased from Sigma-Aldrich. In previous experiments we used high regio-regularity (>98%) and high M_w (50–90 kDa) P3HT purchased from Plextronics for additive DISC patterning experiments and experienced no

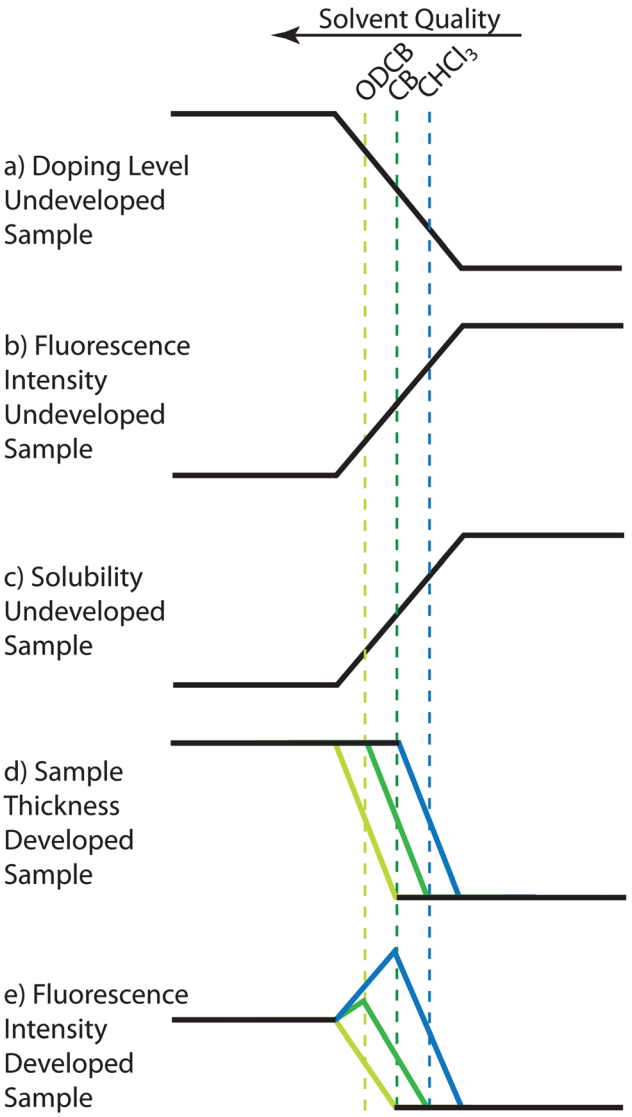

Fig. 7 Summary of findings: this cartoon shows pictorially how the AFM and confocal microscopy data relate at an interface before and after development. (a) shows how the doping level varies across the interface prior to development (like in Fig. 2). (b) shows that fluorescence intensity is inversely proportional to doping level. (c) shows that the P3HT solubility is inversely proportional to doping level. The vertical dotted lines show that ODCB is able to dissolve a less soluble (more highly doped) polymer than either CB or $CHCl_3$. This line depicts that higher solvent quality is related to a more aggressive etch as in Fig. 5. (d) shows the height profile across the developed sample assuming development with ODCB (lt green), CB (dk green), and $CHCL_3$ (blue). The fluorescence intensity of the developed sample is a product of the sample thickness (e) and fluorescence intensity of the undeveloped sample (b) yielding a large peak in fluorescence intensity for $CHCl_3$ and no peak for ODCB, as seen in Fig. 4.

thickness change upon development, even using ODCB as a development solvent.[12] With the lower grade P3HT used here, we show that there is virtually no change in sample thickness upon development using $CHCl_3$ as the development solvent. We can thus conclude that the development solvent quality must be adjusted to the polymer M_w and PDI and that a low PDI polymer is desirable for DISC patterning applications.

In all of the samples depicted so far in this study, the initial P3HT film thickness was kept at 50 ± 1 nm so that we could compare the fluorescence intensities and etch features quantitatively. It leads, however, to the concern that only very thin films can be additively patterned using the DISC process. To address this concern, we additively DISC patterned two different P3HT films. The first film had an initial thickness 240 nm, was spin coated from ODCB, and was developed using ODCB. The second sample had an initial thickness of 280 nm, was spin coated using CB and developed using $CHCl_3$. For both samples, only 3 nm of F4TCNQ was evaporated, so these samples have ~5× lower F4TCNQ concentration per volume as the samples above. Fig. S11 and S12 (ESI†) depict the AFM images and comparison of cross-sections between these thick samples and the thin samples from Sections 1 and 2 that were coated and developed with identical solvents. Fig. 8 summarizes the data by showing cross sections of the thickness normalized to the initial sample thickness and derivatives of the cross sections that allow quantitative comparison between the FWHD of the pattern edge. This data shows several things in general:

1. Thick films can be additively DISC patterned

2. Total layer thickness decreases upon development with reduced doping density

3. The trend in FWHD edge derivatives with coating and development solvents holds for thick films

Specifically, the data shows, that dopants entering a thick film diffuse a broader range of distances, making the pattern edge less sharp. This result suggests that precision patterning of thick films will require dopants that diffuse less readily than F4TCNQ.

Our model for dopant diffusion postulates that the dopants diffuse while neutral until finding a free doping site on the polymer. Once Coulombically bound, the dopant is less likely to diffuse large distances. For the thick samples, a lower doping density was used. This means that volume elements exposed to the dopant have ~5× fewer dopants, which in turn means more available doping sites and less diffusion out of the masked area. When comparing the thick samples to the thin samples, it appears that dopants diffused the same distance because the features are almost identically narrow at zero thickness. However the thicker samples have a much slower change from zero to full thickness with thickness change spanning 10 μm, which can be attributed to a larger gradient of the doping density prior to development. Both samples also show reduction in thickness even within the masked area, which means that prior to development, dopant density was lower around the border of the masked area due to diffusion out of the masked area. Finally, the ODCB/ODCB sample has a narrower FWHD of the derivative than the CB/$CHCl_3$ sample as was the case for thinner samples.

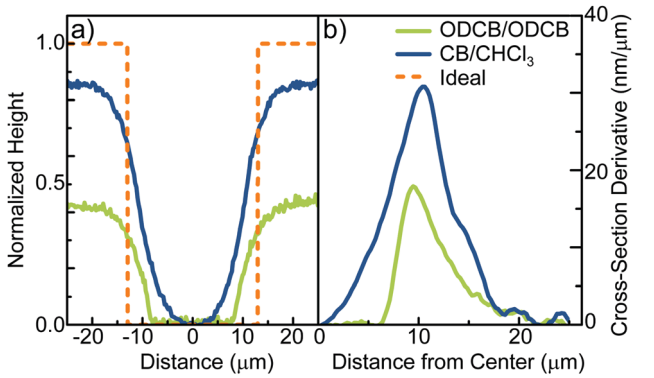

Fig. 8 Thick samples: (a) cross-section of the normalized thickness for a 280 nm sample coated from CB and developed with $CHCl_3$ (dk blue) and a 240 nm sample coated from ODCB and developed with ODCB (lt green). The shape of the masked feature is in orange. (b) Derivative of the etch feature to show distance dependence of the thickness change.

A full analysis of the effects of initial dopant concentration on the developed pattern is beyond the scope of this article as this analysis will require a quantitative diffusion model. We plan to address the issue of diffusion and the initial concentration and distribution of dopants in a future publication.

Finally, we compare additively DISC patterned films that were patterned using two different dopants. 7-methyloxycarbonyl-2,3,5,6-tetrafluoro-7,7,8-tricyanoquinodimethane (F4MCTCNQ) is a structural derivative of F4TCNQ with one cyano group replaced with a methyl ester. In previous publications, we showed that while F4MCTCNQ is a slightly weaker dopant, it is more miscible with P3HT, and more soluble in common solvents.[19] We also directly compared the diffusion rate of F4MCTCNQ to F4TCNQ and found that its bulk diffusion rate is >10× lower.[21] It stands to reason that a dopant with a lower diffusion rate would create an additive DISC pattern that is truer to the mask dimensions because the dopant will diffuse a shorter distance under the mask. To test this hypothesis, we evaporated 3 nm of F4MCTCNQ through our standard shadow mask onto a 50 nm P3HT film coated from CB. We next developed the pattern using CB. Fig. 9 shows a comparison of the cross section and derivative of the cross section for the films coated and developed using CB. Developing the film coated from F4MCTCNQ caused a larger thickness loss, which could be due to the much higher solubility of the F4MCTCNQ in CB. This result implies either:

1. that increasing the solubility of the dopant shifts the equilibrium towards dissolution during development.[28]

2. that since the F4MCTCNQ is a weaker dopant, its binding energy to P3HT is weaker.[19]

The data presented here cannot distinguish between these possibilities.

The other major difference is that F4MCTCNQ did not diffuse as far outside the masked volume as F4TCNQ, making this etched pattern closest to the mask. This result proves the hypothesis that a slower diffusing dopant produces a more accurate pattern. Comparison of the derivatives of the cross-sections shows that the thickness change occurs more abruptly for the F4MCTCNQ sample. In particular the features are sharper near zero and full thickness, which suggests a sharper dopant concentration profile prior to development. Future work should focus on optimization of dopants that diffuse even more slowly to further increase the pattern fidelity.

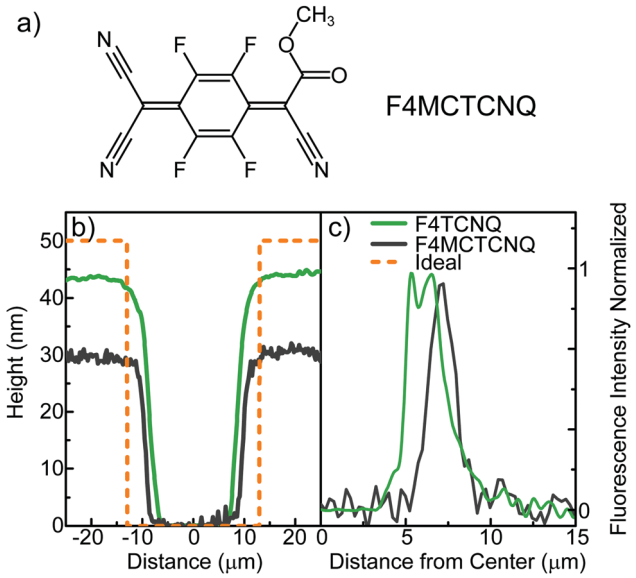

Fig. 9 Comparison of dopants: (a) molecular structure of F4MCTCNQ. (b) Cross section of P3HT films coated from CB, sequentially doped in a pattern with F4TCNQ (green) and F4MCTCNQ (gray), and then developed using CB. (c) Derivative of the cross section to show the sharpness of the pattern.

4 Conclusion

Additive DISC patterning results in lateral features with resolution of 1 μm. The main advantages of additive DISC are that it is operationally very simple and results in patterned features that are much sharper and flatter than from ink jet printing. Standard photo-resists result in sharper features, but we focus here on additive DISC patterning because it enables patterning of polymer semiconductors, which are not compatible with photo-resist processes.

We performed a series of experiments to determine factors that affect the sharpness of additively DISC patterned P3HT samples. The patterning process has two chemical processing steps: sequential doping through a shadow mask *via* dopant evaporation and pattern development *via* immersion in a good solvent for the polymer. We used confocal fluorescence imaging to determine the distribution of dopants in the polymer film prior to development. Analysis of the data shows that dopants diffuse farther outside of the masked area for P3HT samples with increased crystallinity. Our interpretation of this data is that more highly crystalline samples have fewer doping sites available in amorphous domains that can accommodate the presence of a dopant. Crystalline domains are too dense to include dopants in the structure. As a result, the neutral dopants diffuse a greater distance in samples with higher crystallinity.

AFM images of developed samples support the hypothesis that dopants diffuse farther in more highly crystalline samples. The AFM images of developed samples also showed that more sample thickness is lost for better quality development solvents and that these solvents cause a more aggressive etch that is closer to the masked dimensions. There is thus a trade off in choosing the development solvent between a good enough solvent to etch the feature accurately and a poor enough solvent to minimize sample thickness loss. We note that previous studies show that high M_w P3HT with lower PDI also minimizes sample thickness loss.

Analysis of the developed samples using confocal fluorescence microscopy reveals that many of the samples have increased fluorescence at the feature borders where the thickness is reduced. We show that this increased fluorescence is caused by reduced doping density. Each development solvent dissolves P3HT/F4TCNQ to a threshold concentration of F4TCNQ in P3HT. Thus a poor solvent might leave behind very lightly doped P3HT while a good solvent dissolves P3HT/F4TCNQ to a much higher threshold concentration. We show how the initial crystallinity, diffusion, doping level distribution, and solvent quality work together to produce all of the data shown here.

Finally we consider what other factors might affect the pattern fidelity of additively DISC patterned films. To achieve better fidelity, a high M_w and low PDI semiconducting polymer is desired because this puts the polymer in the narrowest solubility window. Additively patterning thick films necessarily leads to poorer pattern fidelity due to more diffusion pathways. We did not consider the concentration of dopants in the initial sequential deposition. Concentration effects and modeling are complex and will be the subject of a future publication. Finally, we examined the effect of a dopant with a lower diffusion rate. Here we show that F4MCTCNQ results in a wider feature that is closer to the mask and a sharper feature edge. Future work will consider co-optimization of initial crystallinity, dopant choice, and development solvent.

Conflicts of interest

There are no conflicts to declare.

Acknowledgements

This project was initiated with funding from the U. S. Department of Energy, Office of Basic Energy Sciences, Division of Materials Sciences and Engineering, under Award No. DE-SC0010419. All data taken on thin films with F4TCNQ were collected with DOE funding. Final experiments involving thick samples and comparison of dopants were carried our under National Science Foundation Award No. 1636385. Z. I. B. V. thanks SENER-CONACyT project no. 291145 for postdoctoral support.

Notes and references

1 H. Sirringhaus, *Adv. Mater.*, 2014, **26**, 1319–1335.
2 O. Bubnova and X. Crispin, *Energy Environ. Sci.*, 2012, **5**, 9345–9362.
3 A. J. C. Kuehne and M. C. Gather, *Chem. Rev.*, 2016, **116**, 12823–12864.
4 F. Liao, M. Zhang, M. Y. Yao, T. Hua, L. Li and F. Yan, *Adv. Mater.*, 2015, **27**, 7493–7527.

5 B. Lüssem, C.-M. Keum, D. Kasemann, B. Naab, Z. Bao and K. Leo, *Chem. Rev.*, 2016, **116**, 13714–13751.
6 J. W. Ward, Z. A. Lamport and O. D. Jurchescu, *ChemPhysChem*, 2015, **16**, 1118–1132.
7 A. C. Arias, J. D. MacKenzie, I. McCulloch, J. Rivnay and A. Salleo, *Chem. Rev.*, 2010, **110**, 3–24.
8 J. A. DeFranco, B. S. Schmidt, M. Lipson and G. G. Malliaras, *Org. Electron.*, 2006, **7**, 22–28.
9 A. A. Zakhidov, J.-K. Lee, J. A. DeFranco, H. H. Fong, P. G. Taylor, M. Chatzichristidi, C. K. Ober and G. G. Malliaras, *Chem. Sci.*, 2011, **2**, 1178–1182.
10 M. C. Gather, A. Köhnen, A. Falcou, H. Becker and K. Meerholz, *Adv. Funct. Mater.*, 2007, **17**, 191–200.
11 D. Bonn, J. Eggers, J. Indekeu, J. Meunier and E. Rolley, *Rev. Mod. Phys.*, 2009, **81**, 739–805.
12 I. E. Jacobs, J. Li, S. L. Berg, D. J. Bilsky, B. T. Rotondo, M. P. Augustine, P. Stroeve and A. J. Moulë, *ACS Nano*, 2015, **9**, 1905–1912.
13 I. E. Jacobs, F. Wang, N. Hazefi, C. Medina-Plaze, T. F. Harrelson, J. Li, M. P. Augustine, M. Mascal and A. J. Moulé, *Chem. Mater.*, 2017, **29**, 832–841.
14 J. Fuzell, I. E. Jacobs, A. Ackling, T. F. Harrelson, D. M. Huang, D. S. Larsen and A. J. Moulé, *J. Phys. Chem. Lett.*, 2016, **7**, 4297–4303.
15 I. E. Jacobs, E. W. Aasen, D. Nowak, J. Li, W. Morrison, J. D. Roehling, M. P. Augustine and A. J. Moulé, *Adv. Mater.*, 2017, **29**, 1603221.
16 A. Dai, A. Wan, C. Magee, Y. Zhang, S. Barlow, S. R. Marder and A. Kahn, *Org. Electron.*, 2015, **23**, 151–157.
17 W. Gao and A. Kahn, *J. Appl. Phys.*, 2003, **94**, 359–366.
18 P. Reiser, L. Müller, V. Sivanesan, R. Lovrincic, S. Barlow, S. R. Marder, A. Pucci, W. Jaegermann, E. Mankel and S. Beck, *J. Phys. Chem. C*, 2018, **122**, 14518–14527.
19 J. Li, G. Zhang, D. M. Holm, I. E. Jacobs, B. Yin, P. Stroeve, M. Mascal and A. J. Moule, *Chem. Mater.*, 2015, **27**, 5765–5774.
20 A. J. Ferguson, N. Kopidakis, S. E. Shaheen and G. Rumbles, *J. Phys. Chem. Lett.*, 2008, **112**, 9865–9871.
21 J. Li, C. Koshnick, S. O. Diallo, S. Ackling, D. Huang, I. E. Jacobs, T. Harrelson, K. Hong, G. Zhang, J. Beckett, M. Mascal and A. J. Moule, *Macromolecules*, 2017, **50**, 5476–5489.
22 M. Al-Ibrahim, O. Ambacher, S. Sensfuss and G. Gobsch, *Appl. Phys. Lett.*, 2005, **86**, 201120.
23 P. K. H. Ho, L. L. Chua, M. Dipankar, X. Y. Gao, D. C. Qi, A. T. S. Wee, J. F. Chang and R. H. Friend, *Adv. Mater.*, 2007, **19**, 215–221.
24 J. Clark, C. Silva, R. H. Friend and F. C. Spano, *Phys. Rev. Lett.*, 2007, **98**, 206406.
25 C. Scharsich, R. H. Lohwasser, M. Sommer, U. Asawapirom, U. Scherf, M. Thelakkat, D. Neher and A. Kohler, *J. Polym. Sci., Part B: Polym. Phys.*, 2012, **50**, 442–453.
26 E. T. Niles, J. D. Roehling, H. Yamagata, A. J. Wise, F. C. Spano, A. J. Moule and J. K. Grey, *J. Phys. Chem. Lett.*, 2012, **3**, 259–263.
27 A. R. Chew, R. Ghosh, Z. R. Shang, F. C. Spano and A. Salleo, *J. Phys. Chem. Lett.*, 2017, **8**, 4974–4980.
28 I. E. Jacobs, J. Li, E. W. Aasen, J. Lopez, T. Fonseca, G. Zhang, P. Stroeve, M. P. Augustine, M. Mascal and A. J. Moule, *J. Mater. Chem. C*, 2016, **4**, 3454–3466.
29 R. J. Kline, M. D. McGehee, E. N. Kadnikova, J. S. Liu and J. M. J. Frechet, *Adv. Mater.*, 2003, **15**, 1519–1522.
30 Y. Kim, S. Cook, S. M. Tuladhar, S. A. Choulis, J. Nelson, J. R. Durrant, D. D. C. Bradley, M. Giles, I. McCulloch, C. S. Ha and M. Ree, *Nat. Mater.*, 2006, **5**, 197–203.
31 M. Koppe, C. J. Brabec, S. Heiml, A. Schausberger, W. Duffy, M. Heeney and I. McCulloch, *Macromolecules*, 2009, **42**, 4661–4666.
32 F. Machui, S. Abbott, D. Waller, M. Koppe and C. J. Brabec, *Macromol. Chem. Phys.*, 2011, **212**, 2159–2165.
33 T. F. Harrelson, Y. Q. Cheng, J. Li, I. E. Jacobs, A. J. Ramirez-Cuesta, R. Faller and A. J. Moulé, *Macromolecules*, 2017, **50**, 2424–2435.